IEEE Access
Multidisciplinary | Rapid Review | Open Access Journal

Received February 23, 2020, accepted March 27, 2020, date of publication April 6, 2020, date of current version April 21, 2020.

Digital Object Identifier 10.1109/ACCESS.2020.2985668

An Anisotropic Traffic Model Based on Driver Interaction

ZAWAR H. KHAN[1], WAHEED IMRAN[2], THOMAS AARON GULLIVER[3], KHURRAM S. KHATTAK[4], ZAHID WADUD[4], AND AKHTAR NAWAZ KHAN[1]

[1]Department of Electrical Engineering, University of Engineering and Technology, Peshawar 25000, Pakistan
[2]National Institute of Urban Infrastructure Planning, University of Engineering and Technology, Peshawar 25000, Pakistan
[3]Department of Electrical and Computer Engineering, University of Victoria, Victoria, BC V8W 2Y2, Canada
[4]Department of Computer System Engineering, University of Engineering and Technology, Peshawar 25000, Pakistan

Corresponding author: Waheed Imran (waheedemran@hotmail.com)

This work was supported by the Higher Education Commission of Pakistan through the establishment of the National Center in Big Data and Cloud Computing at the University of Engineering and Technology, Peshawar.

ABSTRACT The anisotropic Zheng and Jiang models characterize traffic with a constant rearward velocity. They also consider a constant driver sensitivity which can result in unrealistic behavior. In this paper, a new anisotropic model based on a variable rearward velocity is proposed. The transition width, driver reaction, and sensitivity at transitions are used to characterize this velocity. This width impacts traffic alignment with forward conditions and driver reaction can be aggressive, slow or typical. The performance of the proposed, Zheng and Jiang models is evaluated over a 2000 m circular (ring) road with an inactive traffic bottleneck. Results are presented which show that traffic evolution with the proposed model is more realistic than with the Zheng and Jiang models.

INDEX TERMS Anisotropic model, driver reaction, rearward velocity, transition dynamics, Zheng model, Jiang model.

I. INTRODUCTION

Traffic congestion due to reduced road capacity is a major issue in Pakistan [1]. Congestion results in traffic delays, pollution and safety problems [2]–[5]. Knowledge and understanding of traffic flow propagation is essential to effective traffic forecasting and road infrastructure utilization to mitigate congestion. Traffic management strategies should be developed based on realistic traffic flow prediction, for example congestion estimation using traffic flow models [7]–[9]. A key factor affecting this flow is driver reaction to forward stimuli (anisotropic reaction) [10], [11]. However, traffic models based on anisotropic reaction ignore emergency or tail gating vehicles (aggressive drivers). When free flow traffic approaches congestion, velocity variations occur which are known as transition dynamics [12]. The velocity decreases with increasing density and the transition width is defined as the change in density. A small transition width results in small velocity variations and more reactive drivers.

Payne [14] proposed a traffic flow model with an acceleration term based on car following theory. A similar model was independently proposed by Whitham which is based on the indistinguishable behavior of vehicles [15]. The Payne-Whitham (PW) model can be expressed as [16]–[20]

$$\frac{\partial \rho}{\partial t} + \frac{\partial \rho v}{\partial x} = 0, \tag{1}$$

$$\frac{\partial v}{\partial t} + v\frac{\partial v}{\partial x} + \frac{C_0^2}{\rho}\frac{\partial \rho}{\partial x} = \frac{v_e(\rho) - v}{\tau}, \tag{2}$$

where ρ is density and v is velocity. Driver anticipation is given by [21]

$$\frac{C_0^2}{\rho}\frac{\partial \rho}{\partial x},$$

where C_0 is a nonnegative constant which characterizes the spatial density alignment and is typically between 2.4 m/s and 57 m/s [17], [22]. Because vehicle behavior is not uniform, this model can produce unrealistic behavior [23], [24] particularly with large traffic variations [13].

Traffic alignment occurs during the relaxation time τ, after which traffic achieves the equilibrium velocity distribution $v_e(\rho)$. The relaxation term is then given by

$$\frac{v_e(\rho) - v}{\tau}.$$

The associate editor coordinating the review of this manuscript and approving it for publication was Jenny Mahoney.

The convection term

$$\frac{\partial v}{\partial t} + v\frac{\partial v}{\partial x},$$

characterizes the velocity variations due to the ingress and egress of vehicles [21]. Vehicle behavior is influenced by forward vehicles but this is not considered in the PW and associated models [13], [25], which can result in negative velocities with large transition widths [26], [27]. The PW model allows vehicles to move in a direction opposite to the flow, which violates the conditions for traffic flow on a road. With this model, traffic changes in the forward direction can travel at a rate faster than the average velocity. However, these changes should be at a rate slower than the average velocity, which is a characteristic of an anisotropic traffic flow. Zhang [23] improved the PW model by incorporating driver anticipation based on changes in the equilibrium velocity. While this model is anisotropic, a driver adjusts to the traffic density instantaneously and driver physiology is not considered [28]. Another advantage of anisotropic traffic models is that they have low computational complexity [29]–[34].

Aw and Rascle [35] proposed a traffic model in which velocity is a monotonically increasing function of density. This can result in large acceleration and deceleration when the density is high, which is unrealistic [36]. Further, a change in flow can only occur with a change in density.

Jiang *et al.* [6] proposed an anisotropic model which considers driver presumption of forward conditions based on density and spatial changes in velocity. This model is given by

$$\frac{\partial \rho}{\partial t} + \frac{\partial \rho v}{\partial x} = 0, \tag{3}$$

$$\frac{\partial v}{\partial t} + v\frac{\partial v}{\partial x} - C_0\frac{\partial v}{\partial x} = \frac{v_e(\rho) - v}{\tau}, \tag{4}$$

where C_0 is the rearward velocity constant. Thus, changes in upstream traffic propagate with a constant velocity for all transition dynamics, which is impossible. Further, this constant can result in unrealistic behavior with large transition widths. Zheng *et al.* [37] improved the Jiang model by introducing a new relaxation term which gives

$$\frac{\partial \rho}{\partial t} + \frac{\partial \rho v}{\partial x} = 0, \tag{5}$$

$$\frac{\partial v}{\partial t} + (v - C_0)\frac{\partial v}{\partial x} = \zeta\left[\frac{1}{\rho} - \frac{1}{\rho_e(v)}\right], \tag{6}$$

where ζ is the driver sensitivity coefficient and $\rho_e(v)$ is the equilibrium density distribution. However, C_0 and ζ are not based on realistic traffic flow parameters but rather are constants determined based on traffic conditions. Thus, they are not related to the physics of traffic flow.

Driver reaction and time headway characterize traffic propagation. A large reaction is expected when the time headway to align traffic velocities is small. When the response is slow, driver reaction to a stimuli is large to avoid an accident as the transition width is reduced. This is greater when a decelerating stimuli is perceived [56]. Driver reaction to a spatial change in velocity is known as driver sensitivity. For a realistic flow, reaction to stimuli and driver sensitivity should be considered.

In free flow traffic, changes in flow travel downstream (forward) according to the average velocity. During congestion or at transitions, these changes travel upstream (rearward) below the average velocity, which affects driver reaction to forward conditions. Driver reaction to anticipated changes in traffic varies with the conditions. Further, a sensitive driver produces greater acceleration and deceleration which increase the spatial changes in flow. Driver reaction to traffic stimuli at transitions and driver sensitivity characterize the rearward (downstream) velocity propagation. Thus, in this paper a variable rearward velocity based on driver reaction, sensitivity, and traffic stimuli is proposed to characterize traffic flow. This solves the problems with the Zheng and Jiang models. To illustrate this, the performance of the proposed, Jiang and Zheng models is evaluated over a 2000 m circular (ring) road with an inactive traffic bottleneck.

The rest of this paper is organized as follows. The proposed model is presented in Section II and the model decomposition, anisotropy and hyperbolicity are given in Section III. A flow stability analysis is given in Section IV and a traveling wave and shock analysis is presented in Section V. The performance of the proposed, Jiang and Zheng models is investigated in Section VI and some concluding remarks are given in Section VII.

II. PROPOSED TRAFFIC MODEL

Spatial changes in traffic occur at transitions. Vehicle interactions are based on driver sensitivity, response and the stimuli. At traffic changes, drivers align to forward conditions according to the transition velocity v_t which is the product of driver interaction a and relaxation time τ [38]

$$v_t = a\tau. \tag{7}$$

Velocity alignment occurs during the relaxation time. Traffic alignment is quick when vehicle interactions are large and this is denoted by a small value of τ. This is a stimulus for drivers which can be expressed as [28]

$$\left|\frac{dv_e(\rho)}{d\rho}\right| = \left|\frac{d}{d\rho}\left(v_m\left(1 - \frac{\rho}{\rho_m}\right)\right)\right| = \frac{v_m}{\rho_m}, \tag{8}$$

where $v_e(\rho)$ is the equilibrium velocity distribution. The Greenshields equilibrium velocity distribution [39] is typically used and is given by

$$v_e(\rho) = v_m\left(1 - \frac{\rho}{\rho_m}\right), \tag{9}$$

where v_m and ρ_m denote the maximum velocity and maximum density, respectively.

Driver reaction to a stimuli occurs over the transition width. This is smaller in congestion than in free flow traffic due to the larger density. Therefore, the transition width [40] can be

characterized as

$$\delta h = \frac{1}{\delta \rho}, \tag{10}$$

where $\delta\rho$ is the change in density. Velocity changes are greater for larger transition widths as the density is smaller, but the driver stimulus is smaller. Thus stimulus is larger for small transition widths as the conditions are less predictable. Thus, the transition width affects driver reaction and so can be expressed as

$$\frac{1}{\delta \rho}\left|\frac{dv_e(\rho)}{d\rho}\right| = \frac{1}{\delta \rho}\frac{v_m}{\rho_m}. \tag{11}$$

Substituting this in (10) gives

$$\delta h\left|\frac{dv_e(\rho)}{d\rho}\right| = \delta h\frac{v_m}{\rho_m}. \tag{12}$$

The minimum time required to align to forward conditions is $\tau_n = \frac{1}{v_m}$. Thus, for a small change in density, alignment will occur at the maximum speed as a large transition width must be covered and the driver reaction to this stimulus is small. However, as the change in density increases, the transition width decreases. Then driver reaction to a stimulus is larger as a small transition width must be covered during alignment. Therefore, the transition width is a function of the stimulus and is the rate at which the corresponding driver reaction occurs. This is further evidence that a driver is more reactive with a small relaxation time. The minimum relaxation time can be considered is the smallest time between consecutive vehicles to maintain a safe distance (to avoid a collision).

Driver reaction can be characterized as the ratio of reaction time for a typical driver τ to the expected relaxation time τ_a

$$\alpha = \frac{\tau}{\tau_a}. \tag{13}$$

When $\alpha > 1$, i.e. $\tau_a < \tau$, alignment is quicker corresponding to an aggressive driver, whereas a driver is sluggish when $\alpha < 1$, i.e. $\tau_a > \tau$. Driver sensitivity γ [55] can be characterized by the spatial change in velocity during alignment [56]. Driver interaction is then given by the product of (11), (13) and γ

$$a = \frac{\gamma}{\delta \rho}\frac{v_m}{\rho_m}\alpha, \tag{14}$$

where $\delta\rho$ and ρ_m are the changes in normalized density and maximum normalized density, respectively. The normalized density and α are unitless while γ has units $1/\text{s}$ and a has units m/s^2. Substituting (14) in (7) gives

$$v_t = \frac{\gamma}{\delta \rho}\frac{v_m}{\rho_m}\alpha\tau. \tag{15}$$

This indicates that when a driver foresees a change in traffic, velocity is aligned to forward conditions, and is based on the transition width. Changes in traffic propagate downstream (rearward) according to the transition velocity. Therefore, in the proposed model the rearward velocity constant C_0 in the Zheng model is replaced with (15), and the relaxation term is replaced with $\frac{v_e(\rho)-v}{\tau}$ which gives

$$\frac{\partial \rho}{\partial t} + \frac{\partial(\rho v)}{\partial x} = 0, \tag{16}$$

$$\frac{\partial v}{\partial t} + \left(v - \frac{\gamma}{\delta \rho}\frac{v_m}{\rho_m}\alpha\tau\right)\frac{\partial v}{\partial x} = \frac{v_e(\rho)-v}{\tau}. \tag{17}$$

From [41], the distance between vehicles for traffic alignment is $h = \frac{1}{\rho}$, so the distance maintained between vehicles at equilibrium is $h_e = \frac{1}{\rho_e}$. Thus, the relaxation term of the proposed model is a function of h. With this model, driver reaction is based on realistic rearward velocity and relaxation. Conversely, with the Zheng and Jiang models, a driver reacts to changes in traffic conditions based on a constant rearward velocity, which is not realistic.

III. MODEL DECOMPOSITION, ANISOTROPY AND HYPERBOLICITY

The proposed, Zheng and Jiang traffic models are decomposed using the first order centered (FORCE) technique. The spatial and temporal partial derivatives are denoted by the subscripts x and t, respectively. A traffic system in conserved form is given by

$$\psi_t + f(\psi)_x = S(\psi), \tag{18}$$

where ψ is the vector of data variables, i.e. ρ and v. The corresponding functions of the data variables is denoted by $f(\psi)$ and $S(\psi)$ is the vector of source terms [28]. This technique can be used to approximate abrupt changes in traffic flow. The system (18) in quasilinear form is

$$\psi_t + A(\psi)\psi_x = 0, \tag{19}$$

where $A(\psi)$ is the Jacobian matrix which contains the gradients of the functions of variables.

The road length is x_M and there are M equidistant segments so the segment length is $\delta x = x_m/M$. The total time duration is t_N and there are N time steps so a time step is $\delta t = t_N/N$ given by $t_{n+1} - t_n$. ψ and $f(\psi)$ are approximated for the road segments $(x_i + \frac{\delta x}{2}, x_i - \frac{\delta x}{2})$, and the data variables are obtained for each of the M segments for time (t_{n+1}, t_n).

Traffic at the road segment boundaries can be approximated using the FORCE technique [42] which combines the first order Lax-Friedrichs scheme [43] with the second order Richtmyer scheme [44]. This can provide accurate solutions for hyperbolic systems such as (18). Let ψ_i be the average values of the data variables in the ith segment. The flux approximates the change in traffic density and flow at the segment boundary. The flux with the Lax-Friedrichs scheme at the boundary of segments i and $i+1$ in the nth time step is given by

$$\left(f^n_{i+\frac{1}{2}}(\psi^n_i, \psi^n_{i+1})\right)^l = \frac{1}{2}\left(f(\psi^n_i) + f(\psi^n_{i+1})\right) + \frac{1}{2}\frac{\delta t}{\delta x}\left(\psi^n_i - \psi^n_{i+1}\right), \tag{20}$$

where $f(\psi_i^n)$ and $f(\psi_{i+1}^n)$ are the corresponding values of the functions of the data variables in segments i and $i+1$, respectively. The superscript l denotes the Lax-Friedrichs scheme. The data variables obtained with the Richtmyer scheme are [44]

$$\psi_{i+\frac{1}{2}}^n = \frac{1}{2}\left(\psi_i^n + \psi_{i+1}^n\right) + \frac{1}{2}\frac{\delta t}{\delta x}\left(f(\psi_i^n) - f(\psi_{i+1}^n)\right), \tag{21}$$

and the corresponding flux is

$$(f_{i+\frac{1}{2}}^n(\psi_i^n, \psi_{i+1}^n))^r = f(\psi_{i+\frac{1}{2}}^n), \tag{22}$$

where the superscript r denotes the Richtmyer scheme. The flux at the segment boundaries is obtained by averaging (20) and (22) which gives

$$f_i^{n+1} = \frac{1}{2}\left((f_{i+\frac{1}{2}}^n)^r + (f_{i+\frac{1}{2}}^n)^l\right). \tag{23}$$

This approximates the change in density and flow without considering the source. The source terms of the proposed model in (16) and Jiang model in (4) is

$$S(\psi_i^n) = \begin{pmatrix} \frac{v_e(\rho_i^n) - v_i^n}{\tau} \end{pmatrix}, \tag{24}$$

and the source term of the Zheng model in (6) is

$$S(\psi_i^n) = \zeta\left(\frac{1}{\rho_i^n} + \frac{1}{\rho_e(v_i^n)}\right). \tag{25}$$

The updated data variables are obtained by including the source term which gives

$$\psi_i^{n+1} = \psi_i^n - \frac{\delta t}{\delta x}\left(f_{i+\frac{1}{2}}^n - f_{i-\frac{1}{2}}^n\right) + \delta t S(\psi_i^n). \tag{26}$$

If a perturbation (change in flow) propagates with a finite velocity, then the model is hyperbolic. Thus, the effect of a perturbation decreases over time. A traffic model is strictly hyperbolic if the eigenvalues are real and distinct [28]. Anisotropy requires that velocity changes are not greater than the average [45]. The eigenvalues are obtained from the Jacobian matrix to determine anisotropy and hyperbolicity. To construct the Jacobian matrix, a model is considered in conservation form. The Zheng model [37] is given by

$$\psi = \begin{pmatrix} \rho \\ v \end{pmatrix}_t, f(\psi) = \begin{pmatrix} \rho v \\ (\frac{1}{2}v^2 - C_0 v) \end{pmatrix}_x,$$
$$S(\psi) = \begin{pmatrix} 0 \\ \zeta\left[\frac{1}{\rho} - \frac{1}{\rho_e(v)}\right]\rho \end{pmatrix}. \tag{27}$$

For the Jiang model [6], ψ and $f(\psi)$ are the same as in (27), and the source term $S(\psi)$ is given by (25).

The rearward velocity depends on the density change at a transition, driver sensitivity and driver reaction. Therefore, the rearward velocity term is $\frac{\gamma}{\delta\rho}\frac{v_m}{\rho_m}\alpha\tau$, so the proposed model in conservation form is

$$\psi = \begin{pmatrix} \rho \\ v \end{pmatrix}_t, f(\psi) = \begin{pmatrix} \rho v \\ (\frac{1}{2}v^2 - \frac{\gamma}{\delta\rho}\frac{v_f}{\rho_m}\alpha\tau v) \end{pmatrix}_x,$$
$$S(\psi) = \begin{pmatrix} 0 \\ \left(\frac{v_e(\rho) - v}{\tau}\right) \end{pmatrix}. \tag{28}$$

The Jacobian matrix of the Zheng and Jiang models is

$$A(\psi) = \begin{pmatrix} v & \rho \\ 0 & v - C_0 \end{pmatrix}, \tag{29}$$

and the corresponding eigenvalues are

$$\lambda_1 = v - C_0, \lambda_2 = v. \tag{30}$$

These eigenvalues are real and distinct so the model is hyperbolic. The models are anisotropic as changes in traffic are at or below the average speed and are affected by the rearward velocity. However, these changes are based on a constant C_0 for all conditions, which is not realistic. The Jacobian matrix of the proposed model is

$$A(\psi) = \begin{pmatrix} v & \rho \\ 0 & v - \frac{\gamma}{\delta\rho}\frac{dv(\rho)}{d\rho}\alpha\tau \end{pmatrix}, \tag{31}$$

and the corresponding eigenvalues are

$$\lambda_1 = v - \frac{\gamma}{\delta\rho}\frac{dv(\rho)}{d\rho}\alpha\tau, \lambda_2 = v. \tag{32}$$

Changes in traffic are at or below the average velocity, so the anisotropic property is satisfied. Further, the eigenvalues are real and distinct, so the proposed model is hyperbolic. Note that during free flow, traffic perturbations evolve according to λ_2 in the forward direction, while during congestion, they evolve according to λ_1 in the rearward direction.

IV. FLOW STABILITY ANALYSIS

In this section, the stability of the proposed and Jiang models is analyzed. The initial density distribution ρ_0 at $t = 0$ is assumed to be stable and the corresponding velocity $v_o = v(\rho_0)$ is at equilibrium [46], [47]. These assumptions are made to determine the unstable conditions when acceleration and deceleration occur. The disturbances in velocity and density are denoted by v_0 and ρ_0, respectively. The corresponding changes in velocity and density are

$$\Delta\rho = \rho - \rho_0,$$
$$\Delta v = v - v_0. \tag{33}$$

These changes can be expressed as [46]

$$\Delta\rho = \rho_0 e^{ik(x)+w(t)},$$
$$\Delta v = v_0 e^{ik(x)+w(t)}, \tag{34}$$

where $i = \sqrt{-1}$ and $k(x)$ represents spatial changes having units m^{-1}. Since $e^{ik(x)} = \cos k(x) + i\sin k(x)$, traffic is a periodic function of $k(x)$. The temporal changes in density and velocity are given by $\rho_0 e^{w(t)}$ and $v_0 e^{w(t)}$, respectively, with amplification term $w(t)$.

From (1), (2) and (15), the proposed model is

$$\frac{\partial \rho}{\partial t} + \frac{\partial (\rho v)}{\partial x} = 0, \tag{35}$$

$$\frac{\partial v}{\partial t} = -\left(v - \frac{\gamma}{\delta \rho}\frac{dv(\rho)}{d\rho}\alpha\tau\right)\frac{\partial v}{\partial x} + \left(\frac{\partial v(\rho) - v}{\tau}\right) \tag{36}$$

For simplicity, let $\varphi = \frac{\gamma}{\delta\rho}\frac{dv(\rho)}{d\rho}\alpha\tau$, and substituting (33) in (35) and (36) gives

$$\frac{\partial \Delta\rho}{\partial t} + v\frac{\partial \Delta\rho}{\partial x} + \rho\frac{\partial \Delta v}{\partial x} = 0, \tag{37}$$

$$\frac{\partial \Delta v}{\partial t} = -(v-\varphi)\frac{\partial \Delta v}{\partial x} + \left(\frac{v(\rho) - v}{\tau}\right). \tag{38}$$

The spatial changes in density and velocity at a transition from (34) are

$$\begin{aligned}
\frac{\partial \Delta\rho}{\partial x} &= \mathrm{i}k\rho_0 \mathrm{e}^{(\mathrm{i}k(x)+w(t))},\\
\frac{\partial \Delta\rho}{\partial t} &= w\rho_0 \mathrm{e}^{(\mathrm{i}k(x)+w(t))},\\
\frac{\partial \Delta v}{\partial x} &= \mathrm{i}kv_0 \mathrm{e}^{(\mathrm{i}k(x)+w(t))},\\
\frac{\partial \Delta v}{\partial t} &= wv_0 \mathrm{e}^{(\mathrm{i}k(x)+w(t))}.
\end{aligned} \tag{39}$$

Substituting (39) in (37) and (38) [48] gives

$$J\begin{pmatrix}\Delta\rho\\ \Delta v\end{pmatrix} = \begin{pmatrix}0\\0\end{pmatrix}, \tag{40}$$

where

$$\begin{aligned}
J &= \begin{pmatrix} j_{11} & j_{12}\\ j_{21} & j_{22}\end{pmatrix} \\
&= \begin{pmatrix} (\mathrm{i}kv_0 + w) & \mathrm{i}k\rho_0\\ \frac{v(\rho_0)'}{\tau} & -w + \mathrm{i}k(-v_0+\varphi) - \frac{1}{\tau}\end{pmatrix}.
\end{aligned} \tag{41}$$

Thus, (40) gives

$$\begin{pmatrix} (\mathrm{i}kv_0 + w) & \mathrm{i}k\rho_0\\ \frac{v(\rho_0)'}{\tau} & -w + \mathrm{i}k(-v_0+\varphi) - \frac{1}{\tau}\end{pmatrix}\begin{pmatrix}\rho_0 \mathrm{e}^{(\mathrm{i}k(x)+w(t))}\\ v_0 \mathrm{e}^{(\mathrm{i}k(x)+w(t))}\end{pmatrix} = \begin{pmatrix}0\\0\end{pmatrix}. \tag{42}$$

The system is stable if the variations in flow decrease over time. If $\begin{pmatrix}\Delta\rho\\ \Delta v\end{pmatrix}$ is the solution for the proposed model, then $\det(J) = 0$ [49], so the changes in density and velocity are small and do not grow temporally or spatially. Then

$$w^2 + \left(\frac{1}{\tau} - \mathrm{i}k\varphi + \mathrm{i}2kv_0\right)w - k^2v_0^2 + k^2v_0\varphi + \mathrm{i}\frac{kv_0 + k\rho_0 v(\rho_0)'}{\tau} = 0, \tag{43}$$

which gives

$$w^2 + (\phi_1 + \mathrm{i}\epsilon_1)w + \phi_2 + \mathrm{i}\epsilon_2 = 0, \tag{44}$$

where

$$\begin{aligned}
\phi_1 &= \frac{1}{\tau},\\
\epsilon_1 &= -k\varphi + 2kv_0,\\
\phi_2 &= -k^2v_0^2 + k^2v_0\varphi,
\end{aligned}$$

and

$$\epsilon_2 = \frac{kv_0 + k\rho_0 v(\rho_0)'}{\tau}.$$

The solutions of (44) are

$$w_{\pm} = \frac{-(\phi_1 + \mathrm{i}\epsilon_1) \pm \sqrt{(\phi_1 + \mathrm{i}\epsilon_1)^2 - 4(\phi_2 + \mathrm{i}\epsilon_2)}}{2}. \tag{45}$$

If the real part of w denoted $\mathrm{Re}(w_+)$ is negative, variations in density and velocity will decrease over time so traffic changes do not grow temporally and the flow is stable.

The part of (45) under the radical sign can be expressed as

$$\sqrt{R \pm I} = \sqrt{\frac{(\sqrt{R^2+I^2}+R)}{2}} \pm i\sqrt{\frac{(\sqrt{R^2+I^2}-R)}{2}}, \tag{46}$$

so that

$$\mathrm{Re}\left(\sqrt{\frac{(\phi_1 + i\epsilon_1)^2}{4} - (\phi_2 + i\epsilon_2)}\right) = \sqrt{\frac{(\sqrt{R^2+I^2}+R)}{2}}. \tag{47}$$

The real part of (45) is

$$\mathrm{Re}(w_{\pm}) = -\frac{\phi_1}{2} \pm \sqrt{\frac{1}{2}(\sqrt{R^2+I^2}+R)}, \tag{48}$$

where $R = \frac{(\phi_1^2 - \epsilon_1^2 - 4\phi_2)}{4}$ and $I = \frac{(\phi_1\epsilon_1 - 2\phi_2)}{2}$ [50]. The traffic becomes unstable when $\mathrm{Re}(w_+)$ changes from negative to positive which occurs at

$$-\frac{\phi_1}{2} + \sqrt{\frac{1}{2}(\sqrt{R^2+I^2}+R)} = 0, \tag{49}$$

or

$$\sqrt{\frac{1}{2}(\sqrt{R^2+I^2}+R)} = \frac{\phi_1}{2}. \tag{50}$$

Squaring both sides gives

$$\frac{1}{2}(\sqrt{R^2+I^2}+R) = \frac{\phi_1^2}{4}, \tag{51}$$

which can be expressed as

$$\frac{1}{2}(\sqrt{R^2+I^2}) = \frac{\phi_1^2}{4} - \frac{R}{2}. \tag{52}$$

Squaring both sides gives

$$\frac{1}{4}(R^2+I^2) = \left(\frac{\phi_1^2}{4} - \frac{R}{2}\right)^2. \tag{53}$$

which simplifies to

$$\phi_1^2 R + I^2 = \frac{\phi_1^4}{4}. \tag{54}$$

Substituting the values of R and I gives

$$\phi_1^2\phi_2 - \epsilon_2^2 + \phi_1\epsilon_1\epsilon_2 = 0. \tag{55}$$

Now substituting ϕ_1, ϕ_2, ϵ_1 and ϵ_1, the stability condition is obtained as

$$\rho v(\rho_0)' + \varphi = 0, \tag{56}$$

and using $\varphi = \frac{v_m\alpha\gamma\tau}{\rho_m\delta\rho}$ gives

$$\rho v(\rho_0)' + \frac{v_m\alpha\gamma\tau}{\rho_m\delta\rho} = 0. \tag{57}$$

For stability $\mathrm{Re}(w_+) \leq 0$ so that

$$\rho v(\rho_0)' + \frac{v_m\alpha\gamma\tau}{\rho_m\delta\rho} \geq 0. \tag{58}$$

This condition is satisfied if small changes in velocity occur at transitions. Large changes due to perturbations in the proposed model are stabilized by the rearward velocity term $\frac{v_m\alpha\gamma\tau}{\rho_m\delta\rho}$. For the Jiang model, $\varphi = C_0$, so stability requires that

$$\rho v(\rho_0)' + C_0 \geq 0. \tag{59}$$

Thus, spatial alignment occurs with a uniform response C_0 for all conditions. The relaxation term adjusts large changes in velocity to the equilibrium velocity, which can result in unrealistic and oscillatory traffic flow with the Jiang model.

V. TRAVELING WAVE AND SHOCK ANALYSIS

In this section, the conditions for which the proposed model generates a discontinuity (shock) and traveling wave are derived. Consider a monostable waveform

$$(\rho, v)(x - \omega t),$$

with small changes having uniform speed ω between ρ_l, v_l and ρ_r, v_r where the subscripts l, r denote the left and right states of traffic, respectively. These variables are assumed to be within the minimum and maximum values of density and velocity. Further, it is assumed that a traveling wave exists which can be expressed as

$$X = x - \omega t, \quad \rho(X), \quad v(X), \tag{60}$$

Substituting this in (16) gives

$$\frac{\partial\rho(X)}{\partial t} + \frac{\partial\rho(X)v(X)}{\partial X}. \tag{61}$$

From [51]

$$\frac{\partial\rho(X)}{\partial t} = -\omega\frac{\partial\rho(X)}{\partial X}, \tag{62}$$

and substituting this in (61) we obtain

$$-\omega\frac{\partial\rho(X)}{\partial X} + \frac{\partial\rho(X)v(X)}{\partial X}. \tag{63}$$

Integrating (63) with respect to X gives

$$-w + v(X) + \frac{A}{\rho} = 0, \tag{64}$$

where A is the integration constant. Rearranging gives

$$v(X) = \omega - \frac{A}{\rho}, \tag{65}$$

and taking the partial derivative with respect to X we obtain

$$\frac{\partial v(X)}{\partial X} = \frac{A}{\rho^2}\frac{\partial\rho}{\partial X}. \tag{66}$$

From [51]

$$\frac{\partial v(X)}{\partial t} = -\omega\frac{\partial v(X)}{\partial X}, \tag{67}$$

and substituting this in (17) we have

$$-\omega\frac{\partial v(X)}{\partial X} + \left(v(X) - \frac{\gamma}{\delta\rho}\frac{v_m}{\rho_m}\alpha\tau\right)\frac{\partial v(X)}{\partial X} = \frac{v_e(\rho) - v(X)}{\tau}. \tag{68}$$

Rearranging gives

$$\tau\left(-\omega + \left(v(X) - \frac{\gamma}{\delta\rho}\frac{v_m}{\rho_m}\alpha\tau\right)\right)\frac{\partial v(X)}{\partial X} = v_e(\rho) - v(X), \tag{69}$$

and substituting (65) and (66) and multiplying by ρ results in

$$-\tau(v(X) - \omega)\left(v(X) - \frac{\gamma}{\delta\rho}\frac{v_m}{\rho_m}\alpha\tau - \omega\right)\frac{\partial\rho}{\partial X} = \rho v_e(\rho) - \rho\omega - A. \tag{70}$$

For traveling wave speed ω, the spatial change in density is negligible so that $\frac{\partial\rho}{\partial X} = 0$ and

$$\rho v_e(\rho) - \rho\omega - A = 0, \tag{71}$$

which satisfies

$$\rho_l v_e(\rho) - \rho_l\omega - A = \rho_r v_e(\rho) - \rho_r\omega - A. \tag{72}$$

Then ω between ρ_l and ρ_r is given by

$$\omega = \frac{\rho_r v_e(\rho) - \rho_l v_e(\rho)}{\rho_r - \rho_l}. \tag{73}$$

The flows on the right $\rho_r v_e(\rho)$ and left $\rho_l v_e(\rho)$ are concave functions as $\rho v_e(\rho)'' < 0$, which indicates that $\rho_r < \rho_l$. Thus, there exists a steady compression wave between ρ_l and ρ_r. Concavity ensures that there will be small positive spatial changes in density ($\frac{\partial\rho(X)}{\partial X} > 0$), so then from (70)

$$-\tau(v(X) - \omega)\left(v(X) - \frac{\gamma}{\delta\rho}\frac{v_m}{\rho_m}\alpha\tau - \omega\right) > 0. \tag{74}$$

This inequality is satisfied when

$$v(X) - \frac{\gamma}{\delta\rho}\frac{v_m}{\rho_m}\alpha\tau < \omega < v(X). \tag{75}$$

However, when (74) changes sign such that the spatial change in density is negative ($\frac{\partial\rho(X)}{\partial X} < 0$), there will be a significant change in density which is called a shock (discontinuity).

TABLE 1. Simulation parameters.

Parameter	Value
Simulation time for the proposed, Jiang and Zheng models	10 s
Length of the circular road	2000 m
Maximum velocity	30 m/s
Time step for the proposed, Jiang and Zheng models	0.01 s
Road step for the proposed, Jiang and Zheng models	10 m
Relaxation time	$\tau = 3$ s
Equilibrium velocity distribution $v_e(\rho)$	Greenshields
Maximum normalized density	$\rho_m = 1$
Rearward propagation velocity constant C_0 for the Zheng model	14.969 m/s, 18 m/s and 50 m/s
Relaxation time for an aggressive driver	$\tau_a = 1.5$ s, 2 s
Relaxation time for a sluggish driver	$\tau_a = 10$ s, 30 s
Driver reaction for the proposed model	$\alpha = \frac{\tau}{\tau_a} = 0.1, 0.3, 1.5, 2$
Driver sensitivity coefficient for the Zheng model	$\gamma = 0.011, 0.11$ and 0.090 $(\frac{1}{s^2})$
Transition width	$\delta\rho = 0.79$
Driver sensitivity	$\gamma = 1\ s^{-1}$

VI. PERFORMANCE RESULTS

In this section, the performance of the proposed, Jiang and Zheng models is assessed over a circular (ring) road of length 2000 m. The simulation parameters are given in Table 1. Stability is guaranteed by employing the Courant, Friedrich and Lewy (CFL) stability conditions [52]. The corresponding road and time steps for the three models are 10 m and 0.01 s, respectively. The total simulation time for the models is 10 s. The maximum velocity is $v_m = 30$ m/s and the target is Greenshields equilibrium velocity distribution (9). The maximum normalized density is $\rho_m = 1$ which means the road is 100% occupied, and the transition width is $\delta\rho = 0.79$. The relaxation time is set to $\tau = 3$ s as typical values range from 0.5 s to 3 s [53], [54], and γ is chosen as 1 s^{-1}. For the proposed model, $\alpha = 1.5$ and 2 give $\tau_a = 2$ s and 1.5 s which correspond to an aggressive driver, and $\alpha = 0.1$ and $\alpha = 0.3$ give $\tau_a = 10$ s and $\tau_a = 30$ s which correspond to a sluggish driver. The initial density at time $t = 0$ for the models is

$$\rho_0 = \begin{cases} 0.1, & \text{for } x < 1000 \\ 0.8, & \text{for } x \geq 1000 \end{cases} \tag{76}$$

The values of the rearward propagation velocity constant for the Zheng model are $C_0 = 14.969$ and 18 from [37], and $C_0 = 50$ which was chosen to be outside the typical range. The values of γ are 0.011, 0.11 and 0.090 from [37].

The density evolution with the proposed model on a 2000 m circular road at 1 s, 5 s and 10 s with $\alpha = 0.3$ is shown in Figure 1 and the results are tabulated in Table 2. This shows a dense group of vehicles in front of a sparse group. When the sparse group approaches the dense group, a traffic shock wave occurs which travels in the opposite direction of vehicle motion. Conversely, when the dense group approaches the sparse group, vehicles accelerate which creates a low density wave in the direction of vehicle motion. At 1 s, the density is 0.40 at 1 m, and from 60 m to 940 m it is 0.10. It increases to 0.80 at 1070 m and stays at this level until 1940 m. The density is 0.51 at 2000 m. At 5 s, the density is 0.46 at 1 m and decreases to 0.10 at 600 m. It is 0.80 at 1460 m and 0.48 at 2000 m. At 10 s, the density is 0.48 at 1 m and decreases to 0.14 at 660 m. It increases to 0.75 at 1420 m and then decreases to 0.48 at 2000 m.

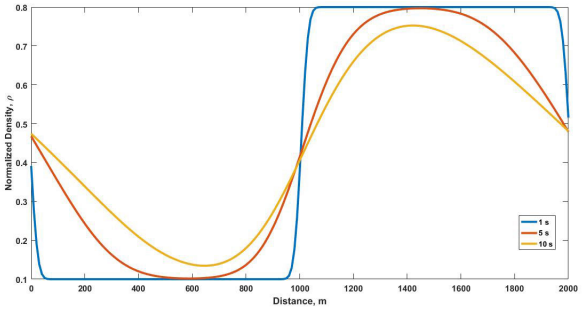

FIGURE 1. Normalized traffic density evolution with the proposed model on a 2000 m circular road with $\alpha = 0.3$ at 1 s, 5 s and 10 s.

TABLE 2. Density and velocity with the proposed model at 1 s, 5 s and 10 s with $\alpha = 0.3$.

Time (s)	Distance (m)	Normalized Density	Velocity (m/s)
1	1	0.40	19.0
1	$60 - 940$	0.10	27.0
1	$1070 - 1940$	0.80	6.0
1	2000	0.51	15.2
5	1	0.46	20.1
5	600	0.10	27.0
5	1460	0.80	6.0
5	2000	0.48	19.7
10	1	0.48	20.5
10	660	0.14	23.7
10	1420	0.75	7.2
10	2000	0.48	20.3

The velocity evolution with the proposed model at 1 s, 5 s and 10 s with $\alpha = 0.3$ is shown in Figure 2 and the results are tabulated in Table 2. At 1 s, the velocity is 19.0 m/s at 1 m and 27.0 m/s between 60 m and 940 m. It decreases to 6.0 m/s at 1070 m and stays at this level until 1940 m. The velocity is 15.2 m/s at 2000 m. At 5 s, the velocity is 20.1 m/s at 1 m and increases to 27.0 m/s at 600 m. It is 6.0 m/s at 1460 m and 19.7 m/s at 2000 m. At 10 s, the velocity increases from 20.5 m/s at 1 m to 23.7 m/s at 660 m. It is 7.2 m/s at 1420 m and increases to 20.3 m/s at 2000 m.

The density evolution with the proposed model on a 2000 m circular road at 1 s, 5 s and 10 s with $\alpha = 1.5$ is shown in Figure 3 and the results are tabulated in Table 3. At 1 s, the density is 0.46 at 1 m, and from 230 m to 790 m it is 0.10. It increases to 0.80 at 1240 m and stays at this level to 1730 m. The density is 0.50 at 2000 m. At 5 s, the density is 0.52 at 1 m, decreases to 0.11 at 490 m, then increases to 0.77 at 1360 m, and is 0.53 at 2000 m. At 10 s, the density is 0.55 at 1 m, decreases to 0.14 at 650 m, and is 0.68 at 1470 m. It is 0.56 at 2000 m.

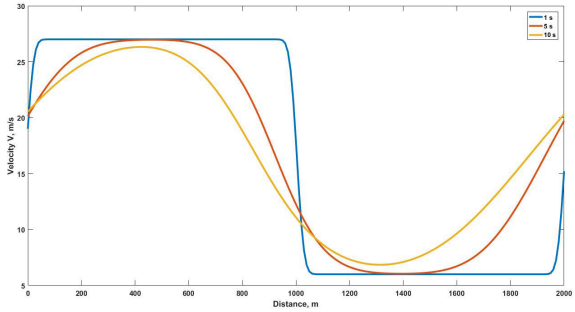

FIGURE 2. Velocity evolution with the proposed model on a 2000 m circular road with $\alpha = 0.3$ at 1 s, 5 s and 10 s.

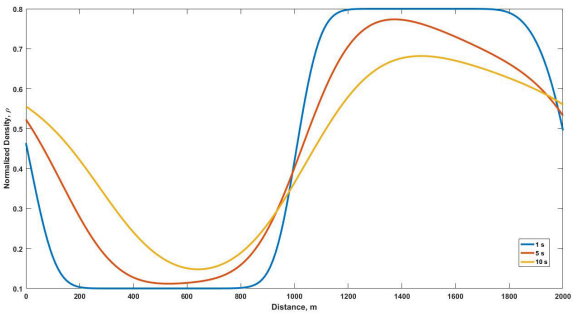

FIGURE 3. Normalized traffic density evolution with the proposed model on a 2000 m circular road with $\alpha = 1.5$ at 1 s, 5 s and 10 s.

TABLE 3. Velocity and density evolution with the proposed model at 1 s, 5 s and 10 s with $\alpha = 1.5$.

Time (s)	Distance (m)	Normalized Density	Velocity (m/s)
1	1	0.46	24.7
1	230 – 790	0.10	27.0
1	1240 – 1730	0.80	6.0
1	2000	0.50	24.1
5	1	0.52	24.4
5	490	0.11	20.0
5	1360	0.77	7.9
5	2000	0.53	24.3
10	1	0.55	18.6
10	650	0.14	11.9
10	1470	0.68	14.5
10	2000	0.56	18.7

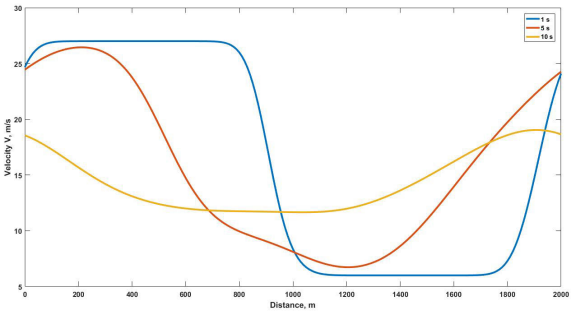

FIGURE 4. Velocity evolution with the proposed model on a 2000 m circular road with $\alpha = 1.5$ at 1 s, 5 s and 10 s.

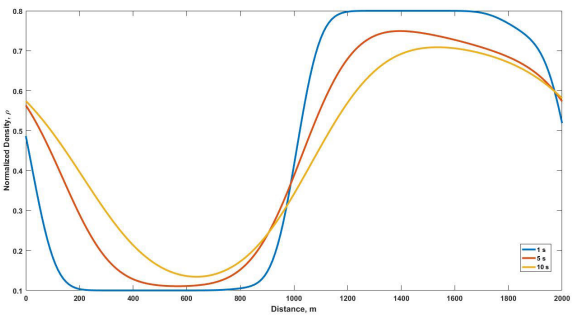

FIGURE 5. Normalized traffic density evolution with the proposed model on a 2000 m circular road with $\alpha = 2$ at 1 s, 5 s and 10 s.

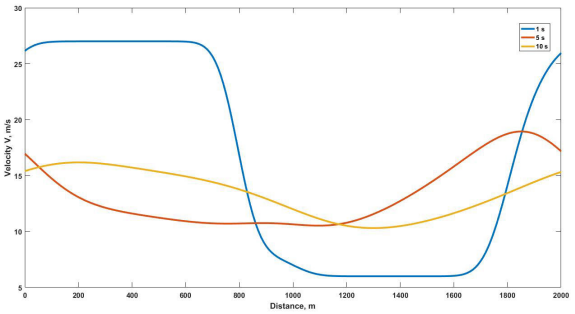

FIGURE 6. Velocity with the proposed model on a 2000 m circular road with $\alpha = 2$ at 1 s, 5 s and 10 s.

The velocity evolution with the proposed model at 1 s, 5 s and 10 s with $\alpha = 1.5$ is shown in Figure 4 and the results are tabulated in Table 3. At 1 s, the velocity is 24.7 m/s at 1 m and is 27.0 m/s between 230 m and 790 m. It decreases to 6.0 m/s at 1240 m and is approximately constant to 1730 m. The velocity is 24.1 m/s at 2000 m. At 5 s, the velocity is 24.4 m/s at 1 m and decreases to 20.0 m/s at 490 m. It is 7.9 m/s at 1360 m and 24.3 m/s at 2000 m. At 10 s, the velocity decreases from 18.6 m/s at 1 m to 11.9 m/s at 650 m. It is 14.5 m/s at 1470 m and increases to 18.7 m/s at 2000 m.

The density evolution with the proposed model at 1 s, 5 s and 10 s with $\alpha = 2$ is shown in Figure 5 and the results are tabulated in Table 4. At 1 s, the density is 0.48 at 1 m and from 270 m to 720 m it is 0.10. It is 0.80 between 1210 m and 1640 m and 0.52 at 2000 m. At 5 s, the density is 0.56 at 1 m, decreases to 0.11 at 600 m, and then increases to 0.75 at 1390 m. It is 0.57 at 2000 m. At 10 s, the density is 0.57 at 1 m, decreases to 0.14 at 660 m, and is 0.70 at 1540 m and 0.58 at 2000 m.

The velocity evolution with the proposed model at 1 s, 5 s and 10 s with $\alpha = 2$ is shown in Figure 6 and the results are tabulated in Table 4. At 1 s, the velocity is 26.2 m/s at 1 m and 27.0 m/s between 270 m and 720 m. It then decreases to 6.0 m/s at 1210 m and stays at this level to 1640 m. The velocity is 26.0 m/s at 2000 m. At 5 s, the velocity is 17.0 m/s at 1 m and decreases to 11.0 m/s at 600 m. It is 12.5 m/s at 1390 m and 17.2 m/s at 2000 m. At 10 s, the velocity decreases from 15.4 m/s at 1 m to 14.6 m/s at 660 m. It is 11.2 m/s at 1540 m and increases to 15.3 m/s at 2000 m.

TABLE 4. Velocity and density evolution with the proposed model at 1 s, 5 s and 10 s with $\alpha = 2$.

Time (s)	Distance (m)	Normalized Density	Velocity (m/s)
1	1	0.48	26.2
1	270 – 720	0.10	27.0
1	1210 – 1640	0.80	6.0
1	2000	0.52	26.0
5	1	0.56	17.0
5	600	0.11	11.0
5	1390	0.75	12.5
5	2000	0.57	17.2
10	1	0.57	15.4
10	660	0.14	14.6
10	1540	0.70	11.2
10	2000	0.58	15.3

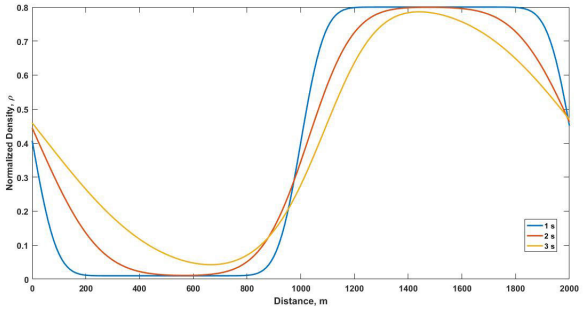

FIGURE 7. Normalized traffic density evolution with the proposed model on a 2000 m circular road with $\alpha = 0.1$ at 1 s, 5 s and 10 s.

The density evolution with the proposed model at 1 s, 5 s and 10 s with $\alpha = 0.1$ is shown in Figure 7 and the results are tabulated in Table 5. At 1 s, the density is 0.40 at 1 m and from 310 m to 730 m it is 0.01. It is 0.80 between 1200 m and 1860 m and 0.45 at 2000 m. At 5 s, the density is 0.45 at 1 m, decreases to 0.01 at 530 m, and then increases to 0.80 at 1420 m. It is 0.79 at 1620 m and decreases to 0.46 at 2000 m. At 10 s, the density is 0.45 at 1 m, decreases to 0.04 at 630 m, and is 0.78 at 1510 m and 0.46 at 2000 m.

The velocity evolution with the proposed model at 1 s, 5 s and 10 s with $\alpha = 0.1$ is shown in Figure 8 and the results are tabulated in Table 5. At 1 s, the velocity is 8.0 m/s at 1 m and 29.0 m/s between 310 m and 730 m. It then decreases to 6.0 m/s at 1200 m and stays at this level to 1860 m. The velocity is 7.8 m/s at 2000 m. At 5 s, the velocity is 11.7 m/s at 1 m and increases to 28.8 m/s at 530 m. It is 6.1 m/s at 1420 m and stays at this level to 1620. It is 11.4 m/s at 2000 m. At 10 s, the velocity increases from 13.6 m/s at 1 m to 30.0 m/s at 630 m. It is 6.6 m/s at 1510 m and increases to 13.1 m/s at 2000 m.

The velocity evolution with the Jiang model on a 2000 m circular road for $C_0 = 14.969$ m/s at 1 s, 5 s and 10 s is shown in Figure 9 and the results are tabulated in Table 6. At 1 s, the velocity is 7.9 m/s at 1 m and is 29.7 m/s between 310 m and 740 m. It decreases to 6.1 m/s at 1200 m and stays at this level to 1870 m. It is 7.7 m/s at 2000 m. At 5 s, the velocity is 11.6 m/s at 1 m and increases to 28.3 m/s at 580 m. It is approximately 6.0 m/s between 1390 m and 1600 m and increases to 11.3 m/s at 2000 m. At 10 s, the velocity increases from 13.1 m/s at 1 m to 29.0 m/s at 620 m. It is 6.5 m/s at 1520 m and increases to 12.9 m/s at 2000 m.

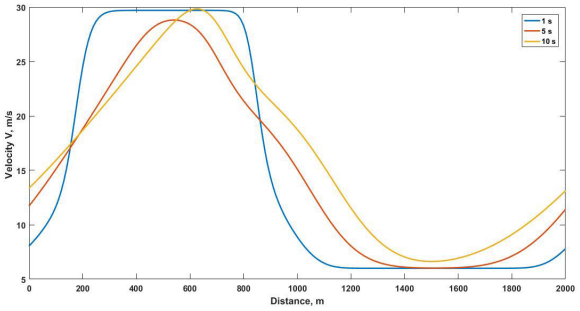

FIGURE 8. Velocity with the proposed model on a 2000 m circular road with $\alpha = 0.1$ at 1 s, 5 s and 10 s.

TABLE 5. Velocity and density evolution with the proposed model at 1 s, 5 s and 10 s with $\alpha = 0.1$.

Time (s)	Distance (m)	Normalized Density	Velocity (m/s)
1	1	0.40	8.0
1	210 – 730	0.01	29.7
1	1200 – 1860	0.80	6.0
1	2000	0.45	7.8
5	1	0.45	11.7
5	530	0.01	28.8
5	1420 – 1620	0.75 – 0.79	6.1
5	2000	0.46	11.4
10	1	0.45	13.6
10	630	0.04	30.0
10	1510	0.78	6.6
10	2000	0.46	13.1

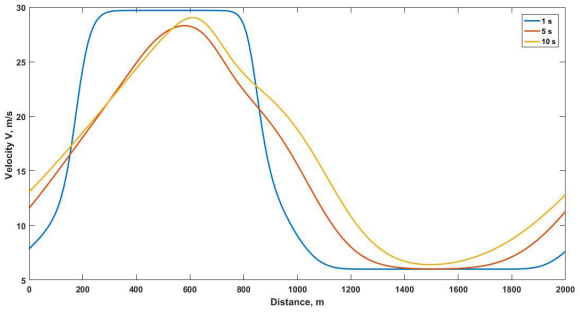

FIGURE 9. Velocity evolution with the Jiang model for $C_0 = 14.969$ m/s on a 2000 m circular road at 1 s, 5 s and 10 s.

The velocity evolution with the Jiang model for $C_0 = 18$ m/s at 1 s, 5 s and 10 s is shown in Figure 10 and the results are tabulated in Table 7. At 1 s, the velocity is 7.7 m/s at 1 m and is 29.7 m/s between 320 m and 740 m. It decreases to 6.0 m/s at 1200 m and is approximately constant to 1800 m. The velocity is 7.5 m/s at 2000 m. At 5 s, the velocity is 11.5 m/s at 1 m and increases to 28.2 m/s at 600 m. It is 6.0 m/s between 1400 m and 1600 m and is 11.2 m/s at 2000 m. At 10 s, the velocity increases from 13.3 m/s at 1 m

TABLE 6. Velocity evolution with the Jiang model at 1 s, 5 and 10 s for $C_0 = 14.969$ m/s.

Time (s)	Distance (m)	Velocity (m/s)
1	1	7.9
1	310 – 740	29.7
1	1200 – 1870	6.1
1	2000	7.7
5	1	11.6
5	580	28.3
5	1390 – 1600	6.0
5	2000	11.3
10	1	13.1
10	620	29.0
10	1520	6.5
10	2000	12.9

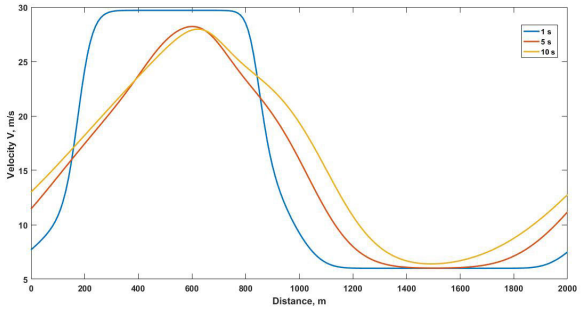

FIGURE 10. Velocity evolution with the Jiang model for $C_0 = 18$ m/s on a 2000 m circular road at 1 s, 5 s and 10 s.

TABLE 7. Velocity evolution with the Jiang model at 1 s, 5 and 10 s for $C_0 = 18$ m/s.

Time (s)	Distance (m)	Velocity (m/s)
1	1	7.7
1	320 – 740	29.7
1	1200 – 1800	6.0
1	2000	7.5
5	1	11.5
5	600	28.2
5	1400 – 1600	6.0
5	2000	11.2
10	1	13.3
10	620	28.0
10	1500	6.4
10	2000	12.8

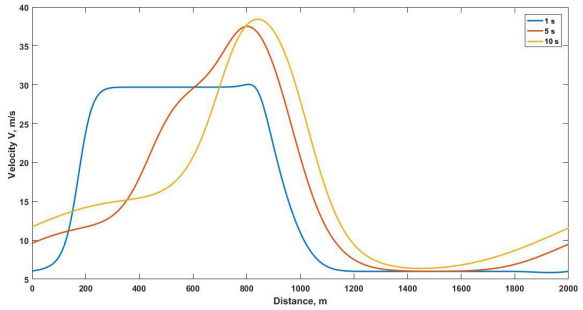

FIGURE 11. Velocity evolution with the Jiang model for $C_0 = 50$ m/s on a 2000 m circular road at 1 s, 5 s and 10 s.

TABLE 8. Velocity evolution with the Jiang model at 1 s, 5 and 10 s for $C_0 = 50$ m/s.

Time (s)	Distance (m)	Velocity (m/s)
1	1	6.0
1	290 – 750	29.7
1	1200 – 1610	6.1
1	2000	7.5
5	1	9.6
5	800	37.7
5	1390 – 1600	6.0
5	2000	9.4
10	1	11.7
10	840	38.5
10	1460	6.4
10	2000	11.6

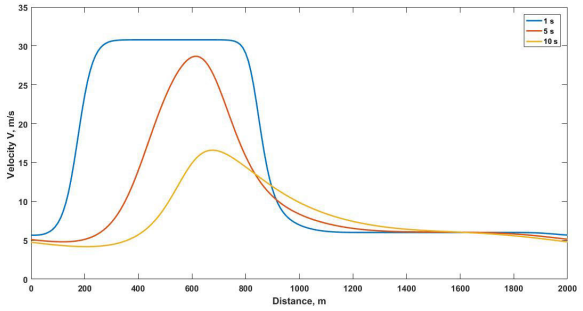

FIGURE 12. Velocity evolution with the Zheng model for $\gamma = 0.011$ and $C_0 = 14.969$ m/s at 1 s, 5 s and 10 s.

to 28.0 m/s at 620 m. It is 6.4 m/s at 1500 m and increases to 12.8 m/s at 2000 m.

The velocity evolution with the Jiang model on a 2000 m circular road for $C_0 = 50$ m/s at 1 s, 5 s and 10 s is shown in Figure 11 and the results are tabulated in Table 8. At 1 s, the velocity is 6.0 m/s at 1 m and is 29.7 m/s between 290 m and 750 m. It decreases to 6.1 m/s at 1200 m and is approximately constant to 1610 m. It is 6.0 m/s at 2000 m. At 5 s, the velocity is 9.6 m/s at 1 m and increases to 37.7 m/s at 800 m. It is approximately 6.0 m/s between 1390 m and 1600 m and increases to 9.4 m/s at 2000 m. At 10 s, the velocity increases from 11.7 m/s at 1 m to 38.5 m/s at 840 m. It is 6.4 m/s at 1460 m and increases to 11.6 m/s at 2000 m.

The velocity evolution with the Zheng model on a 2000 m circular road for $\gamma = 0.011$ and $C_0 = 14.969$ m/s at 1 s, 5 s and 10 s is shown in Figure 12 and the results are tabulated in Table 9. At 1 s, the velocity is 5.7 m/s at 1 m and is 30.0 m/s between 320 m and 730 m. It decreases to 6.2 m/s at 1090 m and then to 5.7 m/s at 2000 m. At 5 s, the velocity is 5.1 m/s at 1 m, increases to 29.0 m/s at 610 m and is 5.1 m/s at 2000 m. At 10 s, the velocity increases from 4.8 m/s at 1 m to 16.6 m/s at 680 m. It is 7.0 m/s at 1260 m and decreases to 4.8 m/s at 2000 m.

The velocity evolution with the Zheng model on a 2000 m circular road for $\gamma = 0.11$ and $C_0 = 14.969$ m/s at 1 s, 5 s and 10 s is shown in Figure 13 and the results are tabulated in Table 10. At 1 s, the velocity is 6.1 m/s at 1 m and is 40.5 m/s between 330 m and 720 m. It decreases to 6.5 m/s at 1060 m and to 6.1 m/s at 2000 m. At 5 s, the velocity is 6.2 m/s at 1 m and increases to 56.5 m/s at 630 m. It is

TABLE 9. Velocity evolution with the Zheng model at 1 s, 5 and 10 s for $\gamma = 0.011$ and $C_0 = 14.969$ m/s.

Time (s)	Distance (m)	Velocity (m/s)
1	1	5.7
1	320 − 730	30.0
1	1090	6.2
1	2000	5.7
5	1	5.1
5	610	29.0
5	2000	5.1
10	1	4.8
10	680	16.6
10	1260	7.0
10	2000	4.8

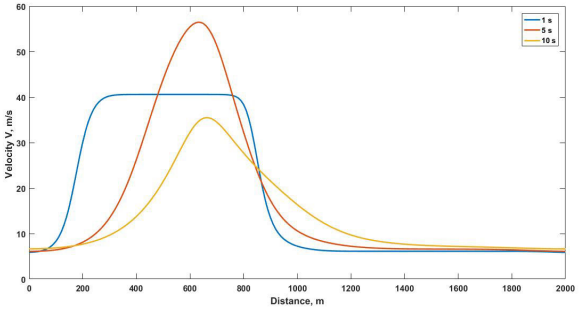

FIGURE 13. Velocity with the Zheng model for $\gamma = 0.11$ and $C_0 = 14.969$ m/s at 1 s, 5 s and 10 s.

TABLE 10. Velocity evolution with the Zheng model at 1 s, 5 and 10 s for $\gamma = 0.11$ and $C_0 = 14.969$ m/s.

Time (s)	Distance (m)	Velocity (m/s)
1	1	6.1
1	330 − 720	40.5
1	1060	6.5
1	2000	6.1
5	1	6.2
5	630	56.5
5	1060	8.9
5	2000	6.2
10	1	6.7
10	670	35.5
10	1170	10.3
10	2000	6.6

8.9 m/s at 1060 m and decreases to 6.2 m/s at 2000 m. At 10 s, the velocity increases from 6.7 m/s at 1 m to 35.5 m/s at 670 m. It is 10.3 m/s at 1170 m and decreases to 6.6 m/s at 2000 m.

The velocity evolution with the Zheng model for $\gamma = 0.011$ and $C_0 = 50$ m/s at 1 s, 5 s and 10 s is shown in Figure 14 and the results are tabulated in Table 11. At 1 s, the velocity is 3.6 m/s at 1 m and is 30.8 m/s between 330 m and 760 m. It decreases to 6.1 m/s at 1150 m and to 3.7 m/s at 2000 m. At 5 s, the velocity is 1.4 m/s at 1 m and increases to 40.7 m/s at 770 m. It is 7.7 m/s at 1160 m and 1.5 m/s at 2000 m. At 10 s, the velocity increases from 0.75 m/s at 1 m to 45.7 m/s at 850 m. It is 6.9 m/s at 1290 m and decreases to 0.80 m/s at 2000 m.

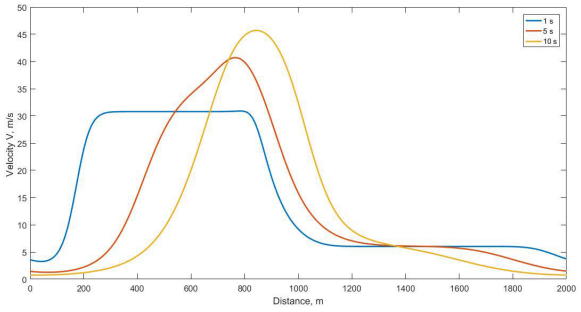

FIGURE 14. Velocity evolution with the Zheng model for $\gamma = 0.011$ and $C_0 = 50$ m/s on a 2000 m circular road at 1 s, 5 s and 10 s.

TABLE 11. Velocity evolution with the Zheng model at 1 s, 5 and 10 s for $\gamma = 0.011$ and $C_0 = 50$ m/s.

Time (s)	Distance (m)	Velocity (m/s)
1	1	3.6
1	330 − 760	30.8
1	1150	6.1
1	2000	3.7
5	1	1.4
5	770	40.7
5	1160	7.7
5	2000	1.5
10	1	0.75
10	850	45.7
10	1290	6.9
10	2000	0.80

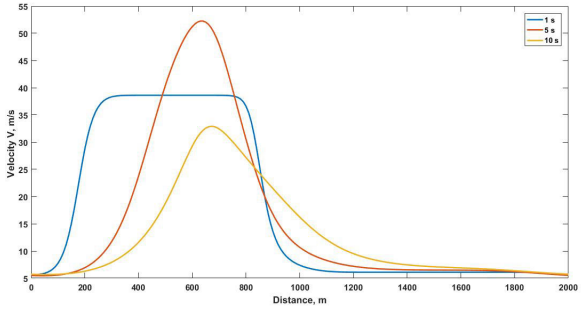

FIGURE 15. Velocity evolution with the Zheng model for $\gamma = 0.090$ and $C_0 = 18$ m/s on a 2000 m circular road at 1 s, 5 s and 10 s.

The velocity evolution with the Zheng model for $\gamma = 0.090$ and $C_0 = 18$ m/s at 1 s, 5 s and 10 s is shown in Figure 15 and the results are tabulated in Table 12. At 1 s, the velocity is 5.7 m/s at 1 m and is 38.6 m/s between 330 m and 710 m. It decreases to 6.8 m/s at 1040 m and to 5.7 m/s at 2000 m. At 5 s, the velocity is 5.5 m/s at 1 m and increases to 52.3 m/s at 630 m. It is 8.0 m/s at 1120 m and 5.5 m/s at 2000 m. At 10 s, the velocity increases from 5.7 m/s at 1 m to 32.9 m/s at 670 m. The velocity is 8.2 m/s at 1290 m and decreases to 5.7 m/s at 2000 m.

The proposed model characterizes traffic flow based on driver reaction and traffic stimuli (driver interaction). The Zheng model characterizes this flow based on a rearward velocity constant C_0 and a constant driver sensitivity γ, which can result in unrealistic traffic behavior. In this section, the Zheng model was evaluated for different values of C_0 and γ. With $C_0 = 14.969$ m/s and $\gamma = 0.011$, the velocity evolution

TABLE 12. Velocity evolution with the Zheng model at 1 s, 5 and 10 s for $\gamma = 0.090$ and $C_0 = 18$ m/s.

Time (s)	Distance (m)	Velocity (m/s)
1	1	5.7
1	330 − 710	38.6
1	1040	6.8
1	2000	5.7
5	1	5.5
5	630	52.3
5	1120	8.0
5	2000	5.5
10	1	5.7
10	670	32.9
10	1290	8.2
10	2000	5.7

is smooth over time as shown in Figure 12. The variations are between 4.8 m/s and 30 m/s which are within range. When γ is increased to 0.11, these variations increase as shown in Figure 13. The velocity reaches 56.5 m/s which exceeds the maximum of 30 m/s. This shows that varying γ in the Zheng model results in unrealistic behavior. With $C_0 = 50$ m/s and $\gamma = 0.011$, the maximum velocity is 45.7 m/s and the minimum is 0.75 m/s as shown in Figure 14. This indicates that increasing C_0 can lead to greater velocity variations. With $C_0 = 18$ m/s and $\gamma = 0.90$ the variations in velocity are again unrealistic as shown in Figure 15. In this case, the velocity reaches a maximum of 52.3 m/s. Thus, the Zheng model cannot be used to characterize different traffic conditions by varying C_0 and γ.

The Jiang model was evaluated for $C_0 = 14.969$ m/s, 18 m/s and 50 m/s. With $C_0 = 14.969$ m/s and 18 m/s, the velocity variations are between 6.0 m/s and 29.7 m/s as shown in Figures 9 and 10 and so are within the minimum and maximum. With $C_0 = 50$ m/s, the velocity reaches 38.5 m/s which exceeds the maximum of 30 m/s. Thus, the Jiang model cannot be used to characterize traffic flow using a constant C_0. This is because it neglects the flow dynamics under different traffic conditions.

The proposed model was evaluated for $\alpha = 0.1$, 0.3, 1.5 and 2. With $\alpha = 0.3$ and 0.1, the evolution of density and velocity are realistic as shown in Figures 1, 2, 7, and 8. The velocity becomes smooth over time and stays within the minimum and maximum. The corresponding results for $\alpha = 1.5$ are shown in Figures 3 and 4, and for $\alpha = 2$ in Figures 5 and 6. These indicate that velocity alignment occurs more smoothly with a larger value of α. In general, the density and velocity with the proposed model evolve realistically over time. Conversely, the Zheng and Jiang models can produce unrealistic results when the traffic conditions are varied.

VII. CONCLUSION

An anisotropic traffic flow model was proposed which characterizes traffic flow based on a variable driver response. The rearward velocity is based on driver reaction, sensitivity and traffic stimuli at transition dynamics. Results were obtained which show that the proposed model characterizes traffic realistically for different conditions, i.e. the velocity evolves smoothly over time and stays within limits. This model can be extended by including the impact of backward driver reaction on the rearward velocity. Further, the stimuli, driver reaction, sensitivity and equilibrium velocity distribution on the road can be considered for different transition widths.

REFERENCES

[1] S. Ye, "Research on urban road traffic congestion charging based on sustainable development," *Phys. Procedia*, vol. 24, pp. 1567–1572, 2012.
[2] K. Chung, J. Rudjanakanoknad, and M. J. Cassidy, "Relation between traffic density and capacity drop at three freeway bottlenecks," *Transp. Res. B, Methodol.*, vol. 41, no. 1, pp. 82–95, Jan. 2007.
[3] K. Yuan, V. L. Knoop, L. Leclercq, and S. P. Hoogendoorn, "Capacity drop: A comparison between stop-and-go wave and standing queue at lane-drop bottleneck," *Transportmetrica B, Transp. Dyn.*, vol. 5, no. 2, pp. 145–158, Apr. 2017.
[4] R. C. Carlson, I. Papamichail, and M. Papageorgiou, "Local feedback-based mainstream traffic flow control on motorways using variable speed limits," *IEEE Trans. Intell. Transp. Syst.*, vol. 12, no. 4, pp. 1261–1276, Dec. 2011.
[5] A. M. Rao and K. R. Rao, "Measuring urban traffic congestion—A review," *Int. J. Traffic Transp. Eng.*, vol. 2, no. 4, pp. 286–305, Dec. 2012.
[6] R. Jiang, Q.-S. Wu, and Z.-J. Zhu, "A new continuum model for traffic flow and numerical tests," *Transp. Res. B, Methodol.*, vol. 36, no. 5, pp. 405–419, Jun. 2002.
[7] B. S. Kerner and S. L. Klenov, "A theory of traffic congestion at moving bottlenecks," *J. Phys. A, Math. Theor.*, vol. 43, no. 42, Oct. 2010, Art. no. 425101.
[8] J. Long, Z. Gao, H. Ren, and A. Lian, "Urban traffic congestion propagation and bottleneck identification," *Sci. China F, Inform. Sci.*, vol. 51, no. 7, pp. 948–964, 2008.
[9] J. A. Laval and L. Leclercq, "A mechanism to describe the formation and propagation of stop-and-go waves in congested freeway traffic," *Phil. Trans. Roy. Soc. A, Math., Phys. Eng. Sci.*, vol. 368, no. 1928, pp. 4519–4541, Oct. 2010.
[10] A. Benyoussef, H. Chakib, and H. Ez-Zahraouy, "Anisotropy effect on two-dimensional cellular-automaton traffic flow with periodic and open boundaries," *Phys. Rev. E, Stat. Phys. Plasmas Fluids Relat. Interdiscip. Top.*, vol. 68, no. 2, Aug. 2003, art. 026129.
[11] Y. Xue and S.-Q. Dai, "Continuum traffic model with the consideration of two delay time scales," *Phys. Rev. E, Stat. Phys. Plasmas Fluids Relat. Interdiscip. Top.*, vol. 68, no. 6, Dec. 2003, Art. no. 066123.
[12] P. Goatin, "The Aw-Rascle vehicular traffic flow model with phase transitions," *Math. Comput. Model.*, vol. 44, nos. 3–4, pp. 287–303, 2006.
[13] C. F. Daganzo, "Requiem for second-order fluid approximations of traffic flow," *Transp. Res. B, Methodol.*, vol. 29, no. 4, pp. 277–286, Aug. 1995.
[14] H. J. Payne, *Models of Freeway Traffic and Control*. Raleigh, NC, USA: Mathematical Models, 1971, pp. 51–61.
[15] G. B. Whitham, *Linear Nonlinear Waves*. New York, NY, USA: Wiley, 1971.
[16] Z. H. Khan, T. A. Gulliver, K. S. Khattak, and A. Qazi, "A macroscopic traffic model based on reaction velocity," *Iranian J. Sci. Technol., Trans. Civil Eng.*, vol. 44, no. 1, pp. 139–150, Mar. 2020.
[17] J. V. Morgan, "Numerical methods for macroscopic traffic models," Ph.D. dissertation, Dept. Math., Univ. Reading, Berkshire, U.K., 2002.
[18] Z. H. Khan and T. A. Gulliver, "A macroscopic traffic model based on anticipation," *Arabian J. Sci. Eng.*, vol. 44, no. 5, pp. 5151–5163, May 2019.
[19] Z. H. Khan, T. A. Gulliver, H. Nasir, A. Rehman, and K. Shahzada, "A macroscopic traffic model based on driver physiological response," *J. Eng. Math.*, vol. 115, no. 1, pp. 21–41, Apr. 2019.
[20] Z. H. Khan, S. A. Ali Shah, and T. A. Gulliver, "A macroscopic traffic model based on weather conditions," *Chin. Phys. B*, vol. 27, no. 7, Jul. 2018, Art. no. 070202.
[21] S. Maerivoet and B. L. R. de Moor, *Transportation Planning and Traffic Flow Models*. Brussels, Belgium: Katholieke Univ. Leuven, 2008.
[22] W. Jin and H. Zhang, "Solving the Payne-Whitham traffic flow model as a hyperbolic system of conservation laws with relaxation," Univ. California Davis, Davis, CA, USA, Tech. Rep. UCD-ITS-Zhang-2001-1, 2001.
[23] H. Zhang, "A theory of non-equilibrium traffic flow," *Transp. Res. B, Methodol.*, vol. 32, no. 7, pp. 485–498, 1998.

[24] Z. H. Khan, "Traffic modelling for intelligent transportation systems," Ph.D. dissertation, Dept. Elect. Comput. Eng., Univ. Victoria, Victoria, BC, Canada, 2016.
[25] A. Hegyi, B. de Schutter, J. Hellendoorn, S. P. Hoogendoorn, and C. Tampère, "Gelijke behandeling voor verkeersstroommodellen," *Verkeerskunde*, vol. 52, pp. 32–36, Jan. 2001.
[26] M. J. Grace and R. B. Potts, "A theory of the diffusion of traffic platoons," *Oper. Res.*, vol. 12, no. 2, pp. 255–275, Apr. 1964.
[27] E. F. Graham and D. C. Chenu, "A study of unrestricted platoon movement of traffic," *Traffic Eng.*, vol. 32, pp. 11–13, 1962.
[28] Z. H. Khan, W. Imran, S. Azeem, K. S. Khattak, T. A. Gulliver, and M. S. Aslam, "A macroscopic traffic model based on driver reaction and traffic stimuli," *Appl. Sci.*, vol. 9, no. 14, p. 2848, 2019.
[29] C. F. Daganzo, "On the variational theory of traffic flow: Well-posedness, duality and applications," *Netw. Heterogeneous Media*, vol. 1, no. 4, pp. 601–619, 2006.
[30] L. Leclercq, J. Laval, and E. Chevallier, "The Lagrangian coordinates and what it means for first order traffic flow models," in *Transportation Traffic Theory*, R. E. Allsop, M. G. H. Bell, B. G. Heydecker, Eds. Oxford, U.K.: Elsevier, 2007, pp. 735–753.
[31] L. Leclercq, J. Laval, and E. Chevallier, "The Lagrangian coordinates applied to the LWR model," in *Hyperbolic Problems: Theory, Numerics, Applications*. Berlin, Germany: Springer, 2007, pp. 671–678.
[32] F. L. M. van Wageningen-Kessels, J. W. C. van Lint, S. P. Hoogendoorn, and C. Vuik, "Implicit and explicit numerical methods for macroscopic traffic flow," in *Proc. Annu. Meeting Transp. Res. Board*, Washington DC, USA, 2009, pp. 9–350.
[33] F. L. M. van Wageningen-Kessels, J. W. C. van Lint, S. P. Hoogendoorn, and C. Vuik, "Implicit time stepping schemes applied to the kinematic wave model in Lagrangian coordinates," in *Proc. Traffic Granular Flow*, Shanghai, China, 2009.
[34] F. L. M. van Wageningen-Kessels, J. W. C. van Lint, S. P. Hoogendoorn, and C. Vuik, "Multiple user classes in the kinematic wave model in Lagrangian coordinates," in *Proc. Traffic Granular Flow*, Shanghai, China, 2009.
[35] A. Aw and M. Rascle, "Resurrection of 'second order' models of traffic flow," *SIAM J. Appl. Math.*, vol. 60, no. 3, pp. 916–938, 2000.
[36] A. D. Richardson, "Refined macroscopic traffic modelling via systems of conservation laws," M.S. thesis, Dept. Math. Statist., Univ. Victoria, Victoria, BC, Canada, 2012.
[37] L. Zheng, Z. He, and T. He, "An anisotropic continuum model and its calibration with an improved monkey algorithm," *Transportmetrica A, Transp. Sci.*, vol. 13, no. 6, pp. 519–543, Jul. 2017.
[38] K. Nagel, P. Wagner, and R. Woesler, "Still flowing: Approaches to traffic flow and traffic jam modeling," *Oper. Res.*, vol. 51, no. 5, pp. 681–710, Oct. 2003.
[39] D. Ni, *Traffic Flow Theory: Characteristics, Experimental Methods, and Numerical Techniques*. Kidlington, U.K: Butterworth-Heinemann, 2016, pp. 55–58.
[40] M. J. Wierbos, V. L. Knoop, F. S. Hänseler, and S. P. Hoogendoorn, "A macroscopic flow model for mixed bicycle-car traffic," *Transportmetrica A, Transp. Sci.*, pp. 1–4, Dec. 2020.
[41] W. Imran, Z. H. Khan, T. Aaron Gulliver, K. S. Khattak, and H. Nasir, "A macroscopic traffic model for heterogeneous flow," *Chin. J. Phys.*, vol. 63, pp. 419–435, Feb. 2020.
[42] E. F. Toro, "On Glimm-related schemes for conservation laws," Dept. Math. Phys., Manchester Metropolitan Univ., Manchester, U.K., Tech. Rep. MMU-9602, 1996.
[43] P. S. J. S. A. S. A. Kachroo Al-nasur Wadoo and A. Shende, *Pedestrian Dynamics: Feedback Control Crowd Evacuation*, New York, NY, USA: Springer, 2008.
[44] R. D. Richtmyer and K. W. Morton, *Difference Methods for Initial-Value Problems*, 2nd ed. New York, NY, USA: Wiley, 1967.
[45] F. van Wageningen-Kessels, B. van't Hof, S. P. Hoogendoorn, H. van Lint, and K. Vuik, "Anisotropy in generic multi-class traffic flow models," *Transportmetrica A, Transp. Sci.*, vol. 9, no. 5, pp. 451–472, May 2013.
[46] D. Helbing and A. F. Johansson, "On the controversy around Daganzo's requiem for and Aw–Rascle's resurrection of second-order traffic flow models," *Eur. Phys. J. B*, vol. 69, pp. 549–562, Sep. 2009.
[47] M. Treiber and A. Kesting, *Traffic Flow Dynamics: Data, Models and Simulation*. Berlin, Germany: Springer, 2013.
[48] A. K. Gupta and I. Dhiman, "Analyses of a continuum traffic flow model for a nonlane-based system," *Int. J. Modern Phys. C*, vol. 25, no. 10, Oct. 2014, Art. no. 1450045.
[49] D. Ngoduy and C. Tampere, "Macroscopic effects of reaction time on traffic flow characteristics," *Phys. Scripta*, vol. 80, no. 2, Aug. 2009, Art. no. 025802.
[50] X. Chen, L. Li, and Q. Shi, "Empirical observations of stochastic and dynamic evolutions of traffic flow," in *Stochastic Evolutions of Dynamic Traffic Flow*. Berlin, Germany: Springer-Verlag, 2015, pp. 27–48.
[51] L. Zheng, P. J. Jin, and H. Huang, "An anisotropic continuum model considering bi-directional information impact," *Transp. Res. B, Methodol.*, vol. 75, pp. 36–57, May 2015.
[52] C. A. de Moura and C. S. Kubrusly, *The Courant-Friedrichs-Lewy (CFL) Condition: 80 Years After its Discovery*, Berlin, Germany: Springer, 2013.
[53] K. Basak, S. N. Hetu, C. L. Azevedo, H. Loganathan, T. Toledo, and M. Ben-Akiva, "Modeling reaction time within a traffic simulation model," in *Proc. 16th Int. IEEE Conf. Intell. Transp. Syst. (ITSC)*, The Hague, The Netherlands, Oct. 2013, pp. 209–302.
[54] P. Yi, J. Lu, Y. Zhang, and H. Lu, "Safety-based capacity analysis for Chinese highways," *IATSS Res.*, vol. 28, no. 1, pp. 47–55, 2004.
[55] R. E. Chandler, R. Herman, and E. W. Montroll, "Traffic dynamics: Studies in car following," *Oper. Res.*, vol. 6, no. 2, pp. 165–184, Apr. 1958.
[56] T. Kim and H. M. Zhang, "Interrelations of reaction time, driver sensitivity, and time headway in congested traffic," *Transp. Res. Rec., J. Transp. Res. Board*, vol. 2249, no. 1, pp. 52–61, Jan. 2011.

ZAWAR H. KHAN received the Ph.D. degree in electrical engineering from the University of Victoria, Victoria, BC, Canada, in 2016.

He is currently an Assistant Professor with the Department of Electrical Engineering, University of Engineering and Technology Peshawar. His research interests include the Internet of Things, traffic analysis, and intelligent transportation systems.

WAHEED IMRAN received the B.Sc. degree in civil engineering from the Wah Engineering College, Wah Cantt, Pakistan, and the M.Sc. degree in urban infrastructure engineering from the National Institute of Urban Infrastructure Planning, University of Engineering and Technology (UET), Peshawar, Pakistan, where he is currently pursuing the Ph.D. degree with the National Institute of Urban Infrastructure Planning.

His research interest includes traffic and transportation engineering.

THOMAS AARON GULLIVER received the Ph.D. degree in electrical engineering from the University of Victoria, Victoria, BC, Canada, in 1989.

From 1989 to 1991, he was employed as a Defence Scientist with Defence Research Establishment Ottawa, Ottawa, ON, Canada. He has held academic appointments at Carleton University, Ottawa, ON, Canada, and the University of Canterbury, Christchurch, New Zealand. He joined the University of Victoria, in 1999, where he is currently a Professor with the Department of Electrical and Computer Engineering. In 2002, he became a Fellow of the Engineering Institute of Canada, and in 2012, a Fellow of the Canadian Academy of Engineering. His research interests include information theory and communication theory, algebraic coding theory, smart grids, intelligent transportation, underwater acoustics, cryptography, and security.

KHURRAM S. KHATTAK received the Ph.D. degree from The George Washington University, Washington, DC, USA, in 2017.

He is currently an Assistant Professor with the Department of Computer Systems Engineering, University of Engineering and Technology, Peshawar. His research interests include intelligent transportation systems, the Internet of Things (IoT), and embedded systems.

ZAHID WADUD received the Ph.D. degree from Comsats University, Pakistan.

He is currently an Assistant Professor with the Department of Computer Systems Engineering, University of Engineering and Technology, Peshawar. His research interests include cellular communication, signal processing, the Internet of Things (IoT), and embedded systems.

AKHTAR NAWAZ KHAN received the Ph.D. degree in electrical engineering from the Asian Institute of Technology, Bangkok, Thailand.

He is currently an Assistant Professor with the Department of Electrical Engineering, University of Engineering and Technology, Peshawar. His research interests include optimization, network communications, and modeling.